ATYPICAL TOPOLOGICAL FEATURES OF THE $Bi_{1-x}Sb_x(0 \leq x \leq 0.2)$ NANO-WIDTH BICRYSTALINE BOUNDARIES

Fiodor M. Muntyanu[1]*, Vitalie Chistol[2], and Elena Condrea[1]**

[1]D.Ghitu Institute of Electronic Engineering and Nanotechnologies, str. Academiei 3/3, Chisinau, 2028 Republic of Moldova
[2]Technical University of Moldova, bulvd. Stefan cel Mare si Sfant 168, Chisinau, 2004 Republic of Moldova
**E-mail: muntean_teodor@yahoo.com*
***E-mail: chistol_vitalie@yahoo.com*

(Received October 4, 2021)

https://doi.org/10.53081/mjps.2021.20-2.02 CZU:538.945+537.622+546.86/87

Abstract

In this paper, we report a number of atypical features of superconductivity, weak ferromagnetism, and quantum transport observed at low temperatures at bicrystalline interfaces of the first predicted and experimentally realized three-dimensional topological insulator (3D TI) $Bi_{1-x}Sb_x$ ($0 \leq x \leq 0.2$). Pure bicrystals and bicrystals slightly doped (≤0.01 at %) with Te (donor) and Sn (acceptor) impurities are used to fully satisfy the conditions of manifestation of transport quantum oscillations. These 3D TI interfaces exhibit fascinating quantum topological properties, which require extensive basic and applied research.
Keywords: bismuth–antimony alloys, bicrystal interface, superconductivity and ferromagnetism.

Rezumat

In presentul articol raportăm o serie de caracteristici atipice ale supraconductibilităţii, feromagnetismului slab și transportului cuantic observate la temperature joase la interfețele bicristaline ale primului izolator topologic tridimensional (3D TI), prezis și realizat experimental in aliajele $Bi_{1-x}Sb_x$ ($0 \leq x \leq 0.2$). Bicristale pure și ușor dopate (≤0.01 at. %) cu impurități deTe (donor) și Sn (acceptor) au fost utilizate pentru a satisface pe deplin condițiile de manifestare a oscilațiilor cuantice de transport. Aceste interfețe 3D TI manifestă proprietăți topologice cuantice fascinante, care necesită cercetări fundamentale și applicate extinse.
Cuvinte cheie: aliaje bismut-antimoniu, interfață bicristal, supraconductivitate și ferromagnetism.

1. Introduction

Bismuth–antimony semiconducting alloys—representatives of the most efficient

thermoelectric materials at low temperatures—are of significant scientific and applied interest [1–3]. We report several topological features of electronic transport and simultaneous manifestation of superconductivity and weak ferromagnetism [4–6] associated with intercrystalline nanoscale interfaces that open up new prospects in the development [7] of various devices (spin injection devices, superconducting/ferromagnetic hybrid structures, thermoelectric devices, etc.).

2. Experimental

The inclination (disorientation angle of $\theta \leq 68^o$) and twisting (disorientation angle of $\theta_1 \leq 75^o$, rotation angle of $\theta_2 \leq 10^o$) $Bi_{1-x}Sb_x$ ($0 \leq x \leq 0.2$) bicrystals were obtained by a modified horizontal zone recrystallization method using the double seed technique and two heaters: one for generating a molten zone and the other for adjusting the temperature gradient ($\Delta T \sim 20^o$C) between the liquid and solid phases. The samples for measurements were composed of two single-crystalline bulk disoriented blocks (crystallites); the superconducting nano-width interface (CI) consisted of a solitary central layer (~60 nm) and two similar adjacent layers (~20-nm-thick each) on both sides of it (Figs. 1a–1c).

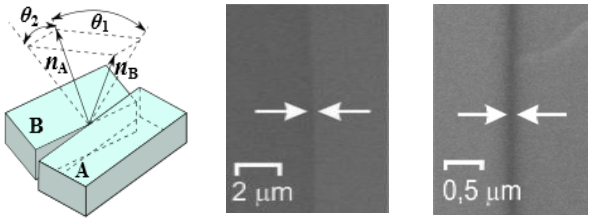

a) b) c)

Fig. 1. (a) Schematic representation of a bicrystal: θ_1, CI disorientation angle; θ_2, CI rotation angle; A and B are crystallites; (b, c) scanning electron microscopy (SEM) images of $Bi_{0.93}Sb_{0.07}Te$ and $Bi_{0.85}Sb_{0.15}Sn$ bicrystals. The arrows indicate the CI location.

The composition of the samples and the residual concentration of magnetic impurities were controlled using a SEM system equipped with Oxford and PV 9800 energy dispersive X-ray (EDX) analyzers, neutron activation analysis, and optical emission spectrometry methods. The superconducting and magnetic properties of the bicrystals were studied in a temperature range of 1.6–300 K using a Quantum Design SQUID magnetometer and a Physical Property Measuring System with a 14-T induction magnet. The quantum oscillations of transport phenomena were registered in stationary and pulse magnetic fields up to 40 T.

3. Results and Discussion

3.1. Superconductivity and weak magnetism

It is well known that, under normal atmospheric conditions, bulk rhombohedral single crystals of $Bi_{1-x}Sb_x$ ($0 \leq x \leq 0.2$) alloys are narrow-band semiconductors; they do not exhibit superconductivity and show anomalous diamagnetism, in common with [1–3]. Contrariwise, one or two new superconducting phases are observed at low temperatures (one has a critical

temperature of T_c~ 8.4–21 K (for different bicrystals); the other, T_c ~ 3.7–4.6 K) [3–5]. Typically, samples with a single superconducting transition were characterized by a high degree of imperfection (Dingle temperature T_D is higher than 3.5 K) and a large crystallite disorientation angle. The zero-field cooled (ZFC) and field cooled (FC) dependences of the magnetic moment *m* denote a considerable Meissner signal, a pronounced flux expulsion, and a superconducting transition starting off at T_{onset}~36 K, which is in good agreement with specific heat data [6]. Estimation of superconducting parameters, especially zero-temperature coherence length ξ(0), indicates that both phases belong to the component layers (central and adjacent) of the bicrystal interfaces, because the crystallites are not superconducting [3]. Three types of magnetic hysteresis loops were identified at inclination and twisting interfaces of $Bi_{1-x}Sb_x$ ($0 \le x \le 0.2$) bicrystals: (i) a symmetrically shaped loop that occurs exclusively against a diamagnetic background typical for strong type-II superconductors (see the upper inset in Fig. 2a); (ii) a ferromagnetic hysteresis loop against a paramagnetic background, which is typical for weak ferromagnetic materials (see the lower inset in Fig. 2a); (iii) a dual loop, i.e., a ferromagnetic and a superimposed superconducting hysteresis loops (see inset of Fig. 2b), which indicates the simultaneous occurrence of superconductivity and weak ferromagnetism.

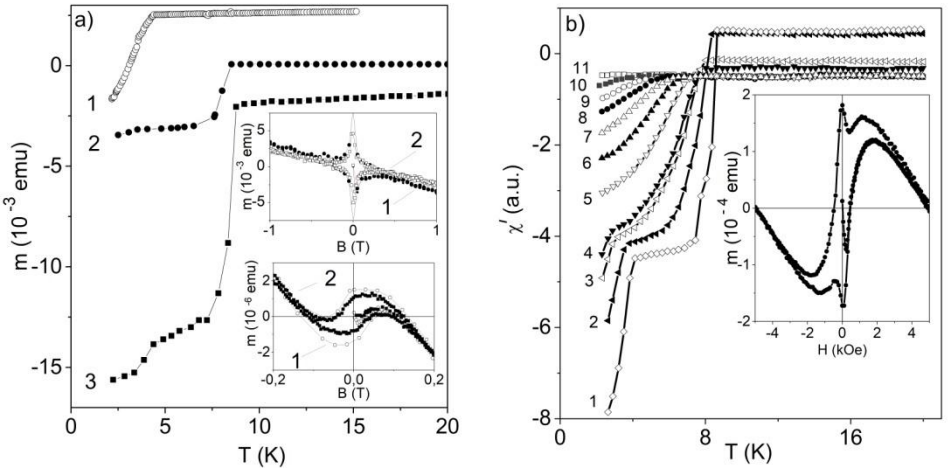

Fig. 2. Magnetic moment *m* and the real part of the AC susceptibility for inclination and twisting bicrystals: **(a)** (*1*) $Bi_{0.94}Sb_{0.06}Te$, θ = 9°, (*2*) $Bi_{0.85}Sb_{0.15}$, θ = 14°, and (*3*) $Bi_{0.94}Sb_{0.06}Te$, θ = 4.6°; the upper inset: a hysteresis loop, $Bi_{0.93}Sb_{0.07}Sn$, θ = 4.6° at 2 and 5 K; the lower inset: a hysteresis loop, $Bi_{0.85}Sb_{0.15}$, θ = 14° at 2 and 10 K; (**b**) $Bi_{0.85}Sb_{0.15}Sn$, θ = 19°, in T: *B* = (*1*) 0, (*2*) 0.04, (*3*) 0.15, (*4*) 0.2, (*5*) 0.4, (*6*) 0.6, (*7*) 0.8, (*8*) 1, (*9*) 1.2, (*10*) 1.5, (*11*) 2; the inset: a hysteresis loop at 1.8 K.

These surprising manifestations of superconductivity and weak magnetism are associated with phonon and electron spectrum modifications; they essentially depend on the disorientation angle of bicrystals and the intensity of interaction of Dirac electrons with impurities and imperfections at the CIs [6].

3.2. Quantum transport anomalies

The study of quantum transport in high magnetic fields makes it possible to detect transitions into a collective state with exceptional quantum properties, reveal the feature of Dirac bands, elucidate the characteristics of fundamental states, and find new possibilities for device

applications [7].

Figures 3a and 3b show typical examples of quantum oscillations of galvano- and thermomagnetic phenomena (longitudinal Hall effect, magnetoresistance, thermomagnetic power) of $Bi_{1-x}Sb_x$ ($0 \le x \le 0.2$) bicrystals. It was found that the oscillating spectrum of quantum transport of these samples, as in the case of Bi bicrystals [2], contains frequencies from the Fermi surface (FS) of the crystallite and two new frequencies associated with FS of the CIs carriers. The oscillations are developed separately in a magnetic field of $B \le 40$ T, and their spectrum is composed of one or two frequencies (manifested at magnetic field different values), which can be determined graphically from the linear dependences of the Landau level index n on the B_n^{-1} position of the oscillation peaks. It was found that, at inclination bicrystals at $1/B_n \to 0$, dependences $n(B_n^{-1})$ are extrapolated to –0.5, as expected for massless Dirac fermions at the CIs, while in twisting bicrystals with a more pronounced degree of imperfection ($3.5 \text{ K} \le T_D \le 9$ K) the interface electronic states are of the Schrödinger type, since n takes integer values. The oscillation frequencies for crystallites can be interpreted in terms of a single-particle picture, while two new harmonics are observed from 2–2.5 T (first frequency) and 10–11 T (second frequency) and exclusively belong to the central and adjacent layers of the CIs, while showing simultaneous weak ferromagnetism and superconductivity.

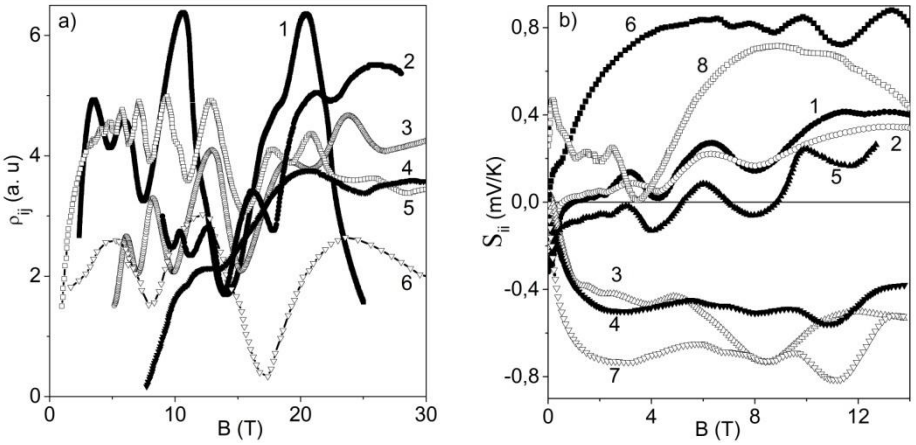

Fig. 3. Examples of quantum transport oscillations for of Bi and $Bi_{1-x}Sb_x$ ($0 \le x \le 0{,}2$) bicrystals: **(a)** (*1*) $\rho_{ii}(B)$, $x = 0.08$, $\theta_1 = 15^o$, $\theta_2 = 3^o$; (*2*) $\rho_{ij}(B_i)$, $x = 0.12$, $\theta_1 = 12^o$, $\theta_2 = 2^o$; (*3*) $\rho_{ii}(B)$, $Bi_{0.93}Sb_{0.07}Te$, $\theta_1 = 19^o$, $\theta_2 = 2^o$; (*4*) $\rho_{ii}(B)$, $x = 0.15$, $\theta_1 = 15^o$, $\theta_2 = 3^o$; (*5*) $\rho_{ii}(B)$, Bi, $\theta = 6^o$; and (*6*) $\rho_{ii}(B)$, $x = 0.1$, $\theta = 6^o$; (**b**) $S_{ii}(B)\Delta T \parallel U$, $B \parallel$ CI plane: (*1*) $\theta = 8^o$, 8.6 K, $x = 0.04$; (*2*) $\theta = 8^o$, 7.6 K, $x = 0.04$; (*3*) $\theta = 7^o$, 4.25 K, Bi; (*4*) $\theta = 8^o$, 6.7 K, $x = 0.11$; (*5*) $\theta = 8^o$, 5.5 K, $x = 0.04$; (*6*) $\theta = 5^o$, 5.2 K, $x = 0.07$; (*7*) $\theta = 4^o$, 6.8 K, $x = 0.09$; and (*8*) $\theta = 68^o$, 5.2 K, $x = 0.07$.

They are highlighted in almost all bismuth–antimony bicrystals regardless of the composition, type of doping, disorientation of crystallites, etc. Moreover, the beginning of these CIs oscillations characterizes almost the same thickness of nanolayers for bismuth, antimony, and bismuth–antimony alloys. The cyclotron mass m/m_e (m_e is the free-electron mass) of electrons, which is assessed from the quantum oscillation amplitude for crystallites and the adjacent and central layers of interfaces of $Bi_{1-x}Sb_x$ ($0 \le x \le 0.2$) bicrystals roughly corresponds to a ratio (in m/m_e units of crystallite carriers) of 1 : 2 : 5. This fact shows that the electron mass in CIs layers is a few times higher than the respective value in crystallites.

A distinct behavior of thermomagnetic power $S_{ii}(B)$ is detected in high fields in bicrystals of 3D Dirac point forming ($x \sim 0.04$): it linearly increases without saturation and the sign changes from negative to positive, which is characteristic of 3D topological semimetals. On the other hand, the $S_{ii}(B)$ dependences in samples with higher antimony concentrations ($0.07 \leq x \leq 0.12$) undergo saturation or increase smoothly (see Fig. 3b), and a nontrivial π-Berry phase was observed in the quantum oscillations of the CI central and adjacent layers; this fact confirms the occurrence of a 3D topological phase. The observed specific features of $S_{ii}(B)$ imply an enhancement in the electronic density of states in a high magnetic field and a decrease in the Fermi energy and contributions of both electron and holes additives to the thermomagnetic power. They are topologically nontrivial, result from the electron–electron interaction [1], and can open promising prospects for a detailed study of topological phase transitions.

Another remarkable high-field feature of magnetoresistance $\Delta\rho(B)/\rho$ is observed in pure $Bi_{1-x}Sb_x$ ($0.08 < x < 0.15$) bicrystals beyond the quantum limit, where the charge carriers occupy only the lowest Landau level ($j = 0$) and the band edge displacement takes place—$\Delta\varepsilon = ½\hbar\omega(1 - \Delta\varepsilon_s/\Delta\varepsilon_o)$—depending on the ratio of spin $\Delta\varepsilon_s$ and orbital level splitting $\Delta\varepsilon_o$. Figure 4 shows examples of high-field dependences of $\Delta\rho/\rho$ in a single crystal and twisting small disorientation angle bicrystals. It is evident that regular Shubnikov–de Haas oscillations are detected up to 2 T and in stronger magnetic fields; charge carriers are beyond the quantum limit. The first maximum at B ~ 8.5 T in the $\Delta\rho(B)/\rho$ dependences for bicrystals (curves *2, 3*) is registered at the same field as for the single crystals (curve *1*). This fact suggests that a semiconductor–semimetal transition is induced in the crystallites [6].

For higher magnetic fields, the second (~11 T) and third additional maxima (~25 T) were revealed. Their occurrence represents a semiconductor–semimetal transition in the adjacent and central layers of the CIs, respectively. Note that the two maxima (second and third) occur at different field values for the bicrystals with various disorientation angles; that is, the transitions occur also at quite different *B* values. This fact suggests that the cyclotron mass of the relevant charge carriers and the $\Delta\varepsilon_s/\Delta\varepsilon_o$ ratio in the crystallites and CI region of the small disorientation angle bicrystals differ considerably, a significant increase in the spin–orbit interaction at the interfaces takes place, and the existence of gapless electronic states at the bicrystal boundary is confirmed. No specific features of $\Delta\rho/\rho$ (see Fig. 4, inset) due to electronic phase transitions of the semiconductor–semimetal type were observed in large disorientation angle bicrystals of $Bi_{1-x}Sb_x$ ($0.08 < x < 0.15$).

Thus, a number of high-field magnetotransport anomalies in $Bi_{1-x}Sb_x$ ($0 \leq x \leq 0.2$) bicrystals with nanoscale multilayer interfaces have been detected. These features do not appear in bulk rhombohedral single-crystalline samples; they are associated with quantum transport manifestations of Dirac carriers at CIs layers, topological changes of their Fermi surface, and the development of some of 3D topological phases of matter.

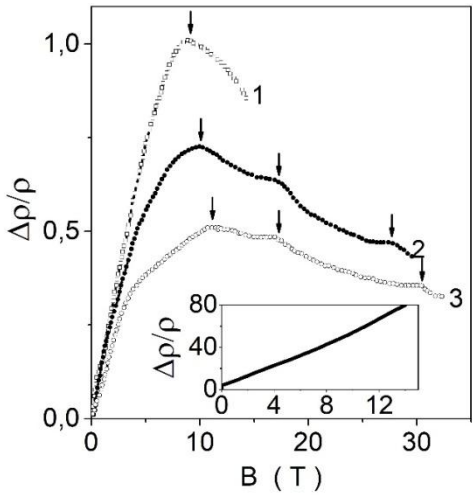

Fig. 4. Semiconductor–semimetal transitions in high magnetic fields in single crystals and bicrystals of $Bi_{1-x}Sb_x$ alloys: (*1*) undoped single crystal, $x = 0.08$; (*2*, *3*) bicrystals: (*2*) $x = 0.08$, $\theta_1 = 4^o$, $\theta_2 = 2^o$ and (*3*) $x = 0.09$, $\theta_1 = 12^o$, $\theta_2 = 2^o$. Arrows indicate the magnetic fields of the semiconductor–semimetal transition; *B* is oriented along the CI plane. Inset: the $Bi_{0.82}Sb_{0.18}$ Sn bicrystal, $\theta_1 = 14^o$, $\theta_2 = 3^o$, 4.2 K.

4. Conclusions

Two superconducting phases with $T_c \leq 21$K and magnetic hysteresis loops against a paramagnetic background indicating the simultaneous occurrence of superconductivity and weak ferromagnetism characteristic of 3D topological insulators have been detected.

The quantum transport in $Bi_{1-x}Sb_x$ ($0.07 \leq x \leq 0.2$) bicrystals is typical for 3D topological insulators, while at $x \sim 0.04$ it shows features of a 3D topological semimetal.

It has been shown that the cyclotron mass of the relevant charge carriers in crystallites and CI layers of the bicrystals differ considerably. A significant increase in the spin–orbit interaction at the bicrystal boundary has been suggested.

References

[1] Jeffrey C.Y. Teo, Liang Fu, and C. L. Kane, Phys. Rev. B78, 045426 (2008).
[2] D. Hsieh, D. Qian, l.Wray, Y. Xia, Y. Hor, R. J. Cava, and M. Z. Hasan, Nature (London) 452, 970 (2008).
[3] F. M. Muntyanu, A. Gilewski, K. Nenkov, J. Warchulska, and A. Zaleski, Phys. Rev. B 73, 132507 (2006).
[4] F. M. Muntyanu, A. Gilewski, K. Nenkov, A. Zaleski, and V. Chistol, Phys. Rev. B 76, 014532 (2007).
[5] F. M. Muntyanu, A. Gilewski, A. J. Zaleski, V. Chistol, and K. Rogacki, Physics Lett. A 381, 2040 (2017).
[6] Fiodor M. Muntyanu, Andrzej Gilewski, Andrzej J. Zaleski, Vitalie Chistol, Viorel Munteanu, Krzysztof Rogacki, and Anatolie Sidorenko, A. Sidorenko (Ed.), Functional Nanostructures and Metamaterials for Superconducting Spintronics, Springer International Publishing AG, 2018, pp.247–263, part of Springer Nature., Resp. ed. A. Sidorenko (Chapter 12).
[7] M.G. Blamire and J. W. A. Robinson, J. Phys.: Condens. Matter. 26, 453201 (2014).